ISSN 0025-6544, Mechanics of Solids, 2009, Vol. 44, No. 5, pp. 792–812. © Allerton Press, Inc., 2009.
Original Russian Text © E.A. Muravleva, L.V. Muravleva, 2009, published in Izvestiya Akademii Nauk. Mekhanika Tverdogo Tela, 2009, No. 5, pp. 164–188.

Unsteady Flows of a Viscoplastic Medium in Channels

E. A. Muravleva* **and L. V. Muravleva****

Lomonosov Moscow State University,
GSP-2, Leninskie Gory, Moscow, 119992 Russia

Received July 24, 2008

Abstract—We numerically study the nonstationary Poiseuille problem for a Bingham–Il'yushin viscoplastic medium in ducts of various cross-sections. The medium acceleration and deceleration problems are solved by using the Duvaut–Lions variational setting and the finite-difference scheme proposed by the authors. The dependence of the stopping time on internal parameters such as density, viscosity, yield stress, and the cross-section geometry is studied. The obtained results are in good agreement with the well-known theoretical estimates of the stopping time. The numerical solution revealed a peculiar characteristic of the stagnant zone location, which is specific to unsteady flows. In the annulus, disk, and square, the stagnant zones arising shortly before the flow cessation surround the entire boundary contour; but for other domains, the stagnant zones go outside the critical curves surrounding the stagnant zones in the steady flow. The steady and unsteady flows are studied in some domains of complicated shape.

DOI: 10.3103/S0025654409050173

Key words: *viscoplastic Bingham-Ilyushin medium, unsteady flow, variational method.*

1. INTRODUCTION

Viscoplastic flow problems attract the attention not only of mechanical engineers but also of mathematicians, numerical analysts, chemists, geophysicists, and rheologists. A comprehensive survey on the topic can be found in the recent papers [1, 2]. In [3], such problems were solved for a more complicated viscoelastoplastic medium. In [4], flows of a viscoplastic fluid in a porous medium were studied.

One of the best known problems is the problem on a viscoplastic flow in a duct. In [5–7], the existence and uniqueness theorems were proved for the solution of the problem on the steady flow in pipes of arbitrary cross-section, and a qualitative investigation of the flow character was performed. The further mathematical study of flow in pipes based on variational inequalities is contained in the monographs [8, 9]. In [10], some exact solutions of the problem of viscoplastic unsteady flow in a circular pipe were obtained for a given law of variation in the core boundary. The numerical simulation of the steady flow in circular and square pipes was performed in [2, 11–15].

A detailed survey of papers published before 2005 and concerned with unsteady flows can be found in [1]. In the recent papers [16–18], the one-dimensional problems of the flow cessation were solved numerically for the plane and axisymmetric Poiseuille flows and the plane Couette flow. In [19, 20], numerical simulation of unsteady modes of the Couette flow in an annular gap was implemented. (This is a one-dimensional problem as well.) Since a detailed survey is not the aim of the present paper, we have noted only the most famous papers.

We consider an unsteady flow of an incompressible viscoplastic medium in a cylindrical pipe with cross-section Ω and boundary Γ under the action of the pressure difference C. It is required to find the velocity v satisfying the equation

$$\begin{aligned} &\rho\frac{\partial v}{\partial t} - \mu\nabla^2 v - \tau_s\nabla\cdot\Big(\frac{\nabla v}{|\nabla v|}\Big) = C \quad \text{in } \Omega\times(0,T),\\ &v = 0 \quad \text{on } \Gamma\times(0,T), \quad v\big|_{t=0} = v_0. \end{aligned} \tag{1.1}$$

*E-mail: catmurav@gmail.ru
**E-mail: lvmurav@gmail.ru

Note that relation (1.1) is not satisfied in the rigid zone $\Omega_0 = \{x \mid x \in \Omega,\ \nabla v(x) = 0\}$.

A characteristic feature of the problems of viscoplastic medium flow is that it is necessary to construct solutions in domains with unknown boundary. This fact is a cause of great difficulties in constructing efficient numerical methods. The main difficulty arises in numerical simulation of the viscoplastic medium flow is due to the singularity of the constitutive relations and to the fact that it is impossible to determine the stresses in the domains where the strain rate is zero. There are two basic groups of methods for overcoming the mathematical difficulties related to the viscoplastic fluid flow. The first of them originates from the regularization methods, which have been widely used for many years. The regularization consists in approximating nondifferentiable constitutive relations by a smooth function for further solving the flow problem for a fluid with nonlinear effective viscosity. For the regularized models, the notion of a rigid zone is not defined, and the condition that a rigid zone exists is introduced by the assumption that the strain rate is small or by the von Mises criterion for stresses ($|\tau| = \tau_s$). This simplified engineering approach sometimes gives an inexact solution, in particular, an incorrect shape of the rigid zones.

2. VARIATIONAL STATEMENT

Another approach may be given by variational methods, which were first proposed for a viscoplastic medium in [21]. The study of flows in pipes in [5–7] is based on the variational approach. The use of the theory of variational inequalities to solve the problems of the Bingham–Il'yushin medium flow is contained in the book [8]. In the monograph [11], some numerical methods for solving the variational inequalities were proposed. They seemed too complicated and did not gain proper acceptance, but recently this approach has become increasingly popular [2, 12–14].

For the time discretization, we use the implicit Euler scheme. Let Δt be a constant time-step. We set $v^0 = v_0$. For $k \geqslant 1$, if v^{k-1} is known, then we find v^k as a solution of the minimization problem for the functional J: $H_0^1(\Omega) \to \mathbb{R}$. It is required to find $v^k \in H_0^1(\Omega)$ such that $J(v^k) \leqslant J(u)$ for all $u \in H_0^1(\Omega)$, where

$$J(u) = \frac{1}{2}\int\limits_\Omega (\alpha|u|^2 + \mu|\nabla u|^2)\,dx + \tau_s \int\limits_\Omega |\nabla u|\,dx - \int\limits_\Omega f u\,dx, \qquad \alpha = \frac{\rho}{\Delta t}, \quad f = C(k\Delta t) + \alpha v^{k-1}. \tag{2.1}$$

In what follows, the superscript k is omitted. The functional (2.1) (for $\alpha = 0$) was introduced in [5] for solving the problem on a standard flow in a pipe.

The main difficulty in solving this problem numerically is due to the fact that the term $\int\limits_\Omega |\nabla v|\,dx$ cannot be differentiated. One of the most successful methods for overcoming this difficulty is the method of Lagrange multipliers [2, 23]. The augmented Lagrangian corresponding to problem (2.1), is determined as follows:

$$L_r(\{v, \mathbf{q}\}, \boldsymbol{\lambda}) = \frac{1}{2}\int\limits_\Omega (\alpha|v|^2 + \mu|\nabla v|^2)\,dx + \tau_s \int\limits_\Omega |\mathbf{q}|\,dx - \int\limits_\Omega f v\,dx + \int\limits_\Omega \boldsymbol{\lambda}\cdot(\nabla v - \mathbf{q})\,dx + \frac{r}{2}\int\limits_\Omega |\nabla v - \mathbf{q}|^2\,dx,$$

where $\mathbf{q}$ has the meaning of the velocity gradient and $\tau_s\boldsymbol{\lambda}$ has the meaning of plastic stresses.

It is proved [23] that solving problem (2.1) is reduced to finding the saddle point $(\{v, \mathbf{q}\}, \boldsymbol{\lambda}) \in (H_0^1(\Omega) \times Q) \times Q$, where $Q \equiv [L^2(\Omega)]^2$, of the Lagrangian L_r and i.e.,

$$L_r(\{v, \mathbf{q}\}, \boldsymbol{\chi}) \leqslant L_r(\{v, \mathbf{q}\}, \boldsymbol{\lambda}) \leqslant L_r(\{u, \boldsymbol{\gamma}\}, \boldsymbol{\lambda}) \quad \forall \{\{u, \boldsymbol{\gamma}\}, \boldsymbol{\chi}\} \in (H_0^1(\Omega) \times Q) \times Q. \tag{2.2}$$

3. SOLUTION ALGORITHM

To find the saddle point of L_r, we use an Uzawa-type algorithm (in the literature, it is often called ALG2 [2, 23]). The algorithm and its implementation are described in detail in [15, 24, 25]. It is one of the versions of the splitting method with respect to physical variables [26]. Each iteration consists of three stages: finding the minimum over velocities, the minimum over the strain rate tensor, and the maximum over stresses. In [15], two finite-difference schemes are proposed and justified for

numerical calculations of steady flows of viscoplastic media. In [24], one of them was used to study the computational aspects arising in solving nonstationary problems (the choice of the step in time and in spatial variables and the stopping criterion). In [15], the problem on the flow cessation in a square pipe was solved numerically. The present paper is a continuation and generalization of the results obtained in [15, 24, 25].

Let us briefly describe this scheme. We consider $\Omega = [0, a] \times [0, b]$ and set $h_1 = a/N_1$ and $h_2 = b/N_2$. We introduce the following grid domains: $\bar{\Omega}_1 = \{x_{ij} = (ih_1, jh_2) \mid i = 0, \ldots, N_1,\ j = 0, \ldots, N_2\}$ and $\bar{\Omega}_2 = \{x_{ij} = ((i + \frac{1}{2})h_1, (j + \frac{1}{2})h_2) \mid i = 0, \ldots, N_1 - 1,\ j = 0, \ldots, N_2 - 1\}$. Let $h_1 = h_2 = h$. The velocity is calculated at the grid nodes Ω_1, and the components of the strain rate and the stress tensors are calculated on the grid Ω_2. In [25], we propose and justify the condition for the discrete problem to be well defined; according to this condition, the Laplace operator is approximated by the "shift" scheme

$$(\Delta_h v_h)_{i,j} = \frac{v_{i-1,j-1} + v_{i+1,j-1} + v_{i+1,j+1} + v_{i-1,j+1} - 4v_{i,j}}{2h^2}.$$

For the discrete operators of gradient and vector divergence, the four-point stencil is used:

$$(\nabla_h v_h)_{i,j} = \frac{v_{i+1,j+1} - v_{i,j+1} + v_{i+1,j} - v_{i,j}}{2h} + \frac{v_{i+1,j+1} - v_{i+1,j} + v_{i,j+1} - v_{i,j}}{2h}$$

$$(\nabla_h \cdot \lambda_h)^1_{i,j} = \frac{\lambda^{11}_{i,j} - \lambda^{11}_{i-1,j} + \lambda^{11}_{i,j-1} - \lambda^{11}_{i-1,j-1}}{2h} + \frac{\lambda^{12}_{i,j} - \lambda^{12}_{i,j-1} + \lambda^{12}_{i-1,j} - \lambda^{12}_{i-1,j-1}}{2h},$$

and similarly, for $(\nabla_h \cdot \lambda_h)^2_{i,j}$.

4. NUMERICAL EXPERIMENTS

4.1. Steady-State Flow

A typical characteristic of viscoplastic medium flows is the existence of a rigid core inside the flow domain and the existence of a critical pressure gradient which must be exceeded permanently to maintain the steady-state flow with a nonzero velocity. As a rule, there are two traditionally considered types of rigid zones: the stagnant zone, where the medium is at rest, and the flow cores, where the medium moves as a rigid body at a constant velocity. As τ_s increases, these zones grow and, for sufficiently large τ_s, block the flow.

The problem of steady-state viscoplastic flow in a pipe of circular cross-section was solved by Buckingham:

$$v(r) = \begin{cases} \dfrac{C(R - r_0)^2}{4\mu}, & 0 \leqslant r \leqslant r_0 \quad \text{(core of flow)}, \\ \dfrac{C(R^2 - r_0^2)}{\mu} - \dfrac{\tau_s(R - r)}{\mu}, & r_0 \leqslant r \leqslant R, \quad r_0 = \dfrac{2\tau_s}{C}. \end{cases}$$

The flow cessation occurs for $r_0 \geqslant R$, i.e., for $\tau_s/C \geqslant \frac{1}{2}R$. The flow has a core of radius $r_0 = 2\tau_s/C$ at the pipe center, and there are no stagnant zones.

For a steady-state flow in an annular pipe (the outer radius is R, and the inner radius is kR), the analytic solution is also known:

$$v(r) = \frac{CR^2}{4\mu} \begin{cases} 2\lambda_1\lambda_2 \ln\dfrac{r}{kR} - \dfrac{r^2}{R^2} + k^2 - 2(\lambda_2 - \lambda_1)\Big(\dfrac{r}{R} - k\Big), & kR \leqslant r \leqslant \lambda_1 R, \\ -2\lambda_1\lambda_2 \ln\dfrac{1}{\lambda_2} - \lambda_2^2 - 2(\lambda_2 - \lambda_1)(1 - \lambda_2), & \lambda_1 R \leqslant r \leqslant \lambda_2 R, \\ -2\lambda_1\lambda_2 \ln\dfrac{R}{r} + 1 - \dfrac{r^2}{R^2} - 2(\lambda_2 - \lambda_1)\Big(1 - \dfrac{r}{R}\Big), & \lambda_2 R \leqslant r \leqslant R. \end{cases}$$

The flow occurs for $C > 2\tau_s/[R(1 - k)]$, the flow core is inside the domain for $\lambda_1 R \leqslant r \leqslant \lambda_2 R$, and there are no stagnant zones.

The medium steady-state flow in a pipe of an arbitrary cross-section was analyzed in [5–7]. It was shown that a necessary and sufficient condition for the flow absence in the domain Ω is the

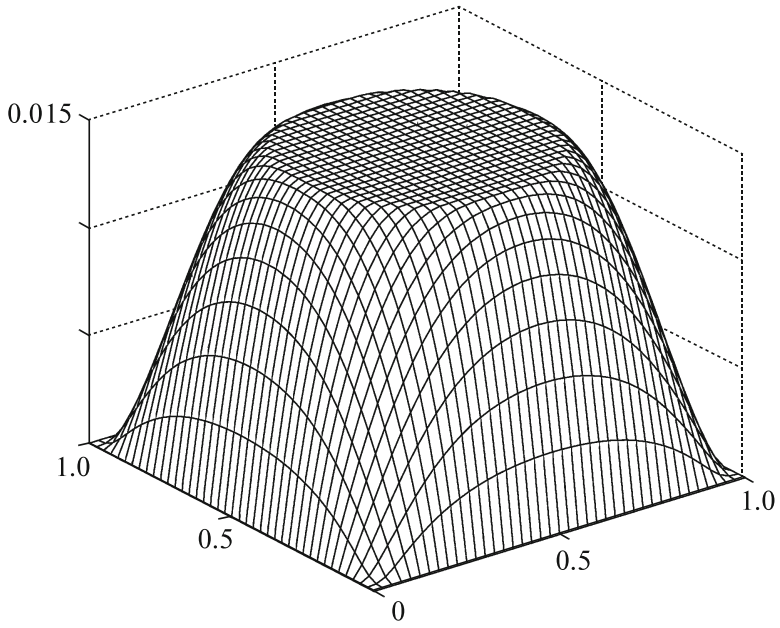

Fig. 1.

condition $C \leqslant \tau_s^{\rm cr}/K$, where $K = \frac{1}{2}R$ for a disk of radius R, $K = \frac{1}{2}(R_1 - R_2)$ for an annulus of outer radius R_1 and inner radius R_2, and

$$K = \frac{a}{2+\sqrt{\pi}}, \quad K = \frac{ab}{a+b+\sqrt{(a-b)^2+\pi ab}}$$

for a square with side a and for a rectangle with sides a and b ($a > b$), respectively. The relation $C^{\rm cr} = \tau_s^{\rm cr}/K$ determines the critical values of the pressure gradient above which the steady-state flow with a nonzero discharge necessarily occurs.

The computed value of $\tau_s^{\rm cr}$ is an important factor characterizing the quality of the obtained numerical solution. The theoretical value for a square with side 2 and for the pressure gradient $C = 1$ is equal to $K = 2/(2+\sqrt{\pi}) \approx 0.5301889$. The value 0.52 was obtained in [14]; the value $K = 0.66$ (which significantly exceeds the theoretical value) was obtained in [13], and a good result, $K = 0.535$, was obtained in [12]. The finite-difference schemes proposed in [15] were used to calculate the value $\tau_s^{\rm cr} = 0.527$; i.e., these results are more sharp than those obtained by other authors by using finite-element approximations. A similar study was also performed for a rectangle of dimensions 2×1. The theoretical value of K is equal to $K = 2/(3+\sqrt{1+2\pi}) \approx 0.350954913$. In computations, the limit value $\tau_s^{\rm cr} = 0.349$ was obtained.

In [5], it was proved that the flow of a viscoplastic medium ($C > C^{\rm cr}$) in a pipe of an arbitrary transverse cross-section always has a core. The flow domain must, at least at some sites, be adjacent to the pipe walls, the boundaries of stagnant zones are always concave towards the stagnant zone and, at each point, have curvature no less than τ_s/C, while the core boundaries at the points of convexity, on the contrary, have curvature no larger than τ_s/C. As τ_s increases, the flow domain between the rigid zones decreases (becomes thinner), and the rigid zones merge at the flow stopping time, while the flow domain degenerates into the critical curve L. For the square and the rectangle, the critical curves L consist of arcs of circles of radius $K = \tau_s^{\rm cr}/C^{\rm cr}$ inscribed in the corners and of intervals of the sides. The stagnant zones of the viscoplastic medium lie outside the domain Ω_L bounded by the critical curve L. A detailed study of the obtained numerical solution of the steady-state zone was performed in [15]. We note that the solution completely corresponds to the theoretical predictions [5–7], and for square cross-sections, is in good agreement with the results obtained in [12–14]. In Fig. 1, we present the volume profile of the velocity for the steady-state flow in a square pipe with side 1 for the pressure gradient $C = 1$ and the yield stress $\tau_s = 0.15$. In Fig. 2, we present the distribution of rigid zones for different values of the yield stress: $(a)\,\tau_s = 0.1$, $(b)\,\tau_s = 0.15$, $(c)\,\tau_s = 0.2$, $(d)\,\tau_s = 0.25$. For all values of τ_s, there flow has a core at

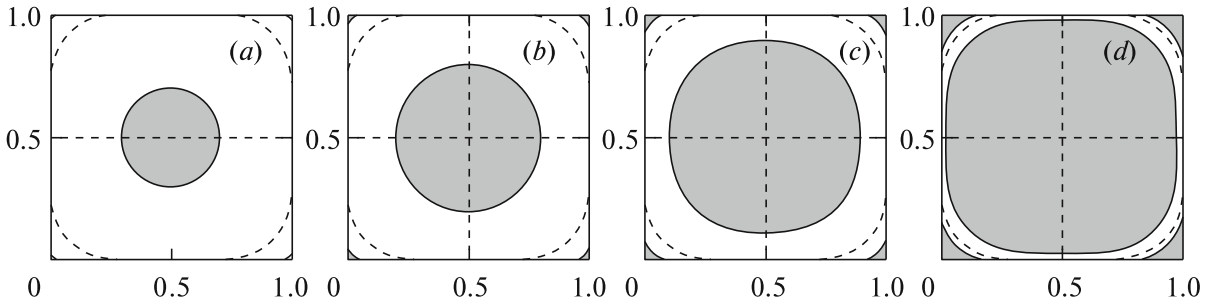

Fig. 2.

Table 1

	$\varepsilon = 1$	$\varepsilon = 2$	$\varepsilon = 3$	$\varepsilon = 4$	$\varepsilon = 5$	$\varepsilon = 6$
$\tau_s = 0.05$	0.02642	0.02091	0.01537	0.01174	0.00932	0.00406
$\tau_s = 0.1$	0.01791	0.01350	0.00914	0.00637	0.00459	0.00112
$\tau_s = 0.15$	0.01008	0.00688	0.00387	0.00213	0.00112	0.00001

the center and stagnant zones at the corners of the square, which are hardly noticeable for $\tau_s = 0.1$. The dashed line is the critical curve L separating the stagnant zones.

The authors believe that the solution of the stationary problem for pipes of rectangular cross-section (including the media with inhomogeneous yield stress) was first obtained in [15].

To study the influence of geometric characteristics, we consider the steady-state flow of a viscoplastic medium in pipes of rectangular cross-section of constant area $S = 1$ and variable side ratio $\varepsilon = W/L$ (W is the width, L is the length, and $WL = S$). In this case, the yield stress $\tau_s = 0.05,\ 0.1,\ 0.15$ and the pressure gradient $C = 1$ are fixed. As was expected, the greatest flow rate corresponds to the square cross-section, and the flow rate decreases as the cross-section elongates. This dependence is illustrated in Table 1.

4.2. Unsteady Flow

An important characteristic of unsteady viscoplastic media flow problems is the finiteness of the decay time interval in the absence of external forces. This is a principal distinction from the corresponding flow of viscous fluid, which exponentially decays in infinite time. A rigorous mathematical justification of this phenomenon was obtained in [22, 23] in the framework of the variational statement.

Theorem [23]. *Let $C = const$ and $T = +\infty$. In this case, if $v_0 \in L^2(\Omega)$, then the following asymptotic behavior takes place: if $C < \tau_s\gamma|\Omega|^{-1/2}$, then*

$$v(t) = 0 \quad \forall t > T_C,$$
$$\gamma = \inf_{u \in H_0^1(\Omega)\setminus\{0\}} \frac{\int\limits_\Omega |\nabla u|\,dx}{\|u\|_{L^2(\Omega)}}, \quad T_C = \frac{\rho}{\mu\lambda_0}\ln\left(1 + \frac{\mu\lambda_0\|v_0\|_{L^2(\Omega)}}{\gamma\tau_s - C|\Omega|^{1/2}}\right), \tag{4.1}$$

where λ_0 is the minimum eigenvalue of the operator $-\Delta$ with the homogeneous Dirichlet boundary conditions ($\lambda_0 > 0$). If $C \geqslant \gamma\tau_s|\Omega|^{-1/2}$, then the estimate

$$\|v(t) - v_\infty\|_{L^2(\Omega)} \leqslant \|v_0 - v_\infty\|_{L^2(\Omega)} \exp\left(-\frac{\mu\lambda_0 t}{\rho}\right) \tag{4.2}$$

holds, where v_∞ is the corresponding steady-state solution.

Moreover, in the proof of this theorem, it was shown that the asymptotic estimate

$$\|v(t)\|_{L^2(\Omega)} + \kappa \leqslant (\|v_0\|_{L^2(\Omega)} + \kappa)\exp\left(-\frac{\mu\lambda_0 t}{\rho}\right), \quad \kappa = \frac{\tau_s\gamma - C|\Omega|^{1/2}}{\lambda_0\mu} \tag{4.3}$$

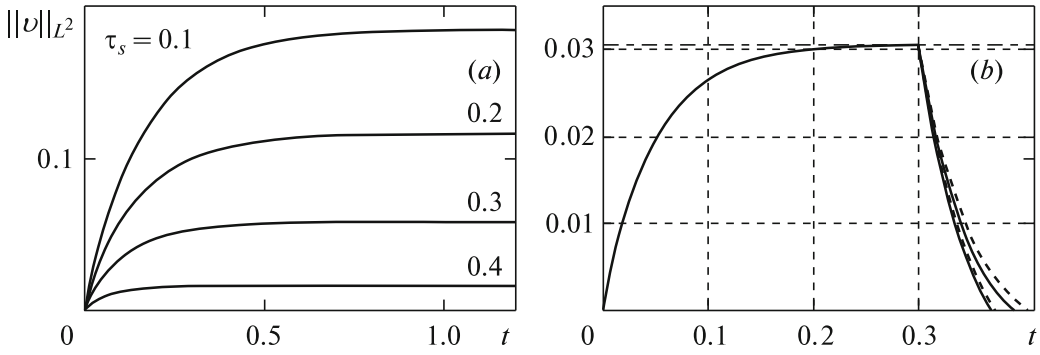

Fig. 3.

is satisfied for $C < \gamma\tau_s|\Omega|^{-1/2}$. Thus, the theorem gives an upper bound for the flow stopping time $T_{\text{stop}} \leqslant T_C$.

This difference scheme was used to perform the numerical simulation of the flow regimes: transition from the rest state to the steady-state regime; the steady-state flow cessation under the condition that the pressure difference is removed instantaneously (i.e., $t = 0$, $C = C_0$, $t > 0$, $C = 0$); the flow cessation under the instantaneous pressure drop to a values lower than the critical value (i.e., $t = 0$, $C = C_0$, $t > 0$, $\partial p/\partial z = C_1$, $C_1 < C^{\text{cr}}$).

4.2.1. Transition to steady-state regime. Consider the problem of start-up of an immovable medium under the action of an instantaneously applied pressure gradient. After a time, the medium practically enters a steady-state regime. As was already noted, the analytic solution is known for a circular pipe in the stationary case, and it is convenient to use this fact to verify the accuracy of the computations. Since $v_0 = 0$, the estimate (4.2) acquires the form

$$\|v(t) - v_\infty\|_{L^2(\Omega)} \leqslant \|v_\infty\|_{L^2(\Omega)} \exp\Big(-\frac{\mu\lambda_0 t}{\rho}\Big) < \delta; \tag{4.4}$$

i.e., it is possible to take a t for which we a priori have $\|v(t) - v_\infty\|_{L^2(\Omega)} < \delta$. Obviously, the larger accuracy we need to achieve, the larger interval must be taken. Since, for the existence of a viscoplastic medium flow in a disk of unit radius with the pressure gradient $C = 1$, the values of the yield stress must lie in the interval $0 < \tau_s < 0.5$, we took the values uniformly distributed over this interval: $\tau_s = 0.1$, $\tau_s = 0.25$, $\tau_s = 0.4$. We considered the time steps from 10^{-3} to $5 \cdot 10^{-6}$. Of course, for smaller time steps the solution is more accurate and approaches the steady-state regime in a smaller time interval. In Table 2, we present the results of numerical computations. All computations were performed with the step in the spatial variables equal to $h = 1/200$ except for the last column ($\varepsilon = 10^{-5}$) for $\tau_s = 0.1$. For this value of τ_s, the norm of the stationary solution $\|v_\infty\|_{L^2(\Omega)}$ for $h = 1/200$ is calculated up to 10^{-5}, and hence this step is insufficient to calculate $\|v_n(t) - v_\infty\|_{L^2(\Omega)} < 10^{-5}$. In this specific case, the computations were performed for $h = 1/500$. The table shows that the estimate is satisfied for all three values of the yield stress; moreover, for $\tau_s = 0.4$, it is satisfied with a great supply, and for the small value $\tau_s = 0.1$, it is very close to the calculated value. In simulations of unsteady flows of a viscoplastic medium, the choice of the time step depends on the yield stress. For $\tau_s = 0.1$, an adequate choice is $\Delta t = 10^{-4}$, and for $\tau_s = 0.4$, it is the step $\Delta t = 10^{-5}$. Figure 3 *a* illustrates the velocity variation in the $L^2(\Omega)$-norm as the medium is accelerated from the immovable state to the steady-state regime for different values of the yield stress.

Consider the flow in a square pipe of unit area. At the initial time moment, the medium is at rest, and then the pressure gradient $C = 1$ is applied instantaneously. In Fig. 3 *b*, this regime corresponds to the time interval $[0, 0.3]$. This piece of the graph illustrates the process of transition to the steady-state flow. The quantity $\|v_\infty\|_{L^2(\Omega)} = 0.030608$ corresponding to $\tau_s = 0.05$ is shown by the dashed line. The value of the calculated velocity $v_h(t)$ approached the steady-state value sufficiently rapidly.

In Table 3, in the first row, we present the calculated values of $\Delta_1(t) = \|v_h(t) - v_\infty\|_{L^2(\Omega)}$, and in the second row, of $\Delta_2(t) = \|v_\infty\|_{L^2(\Omega)} \exp(-\mu\lambda_0 t/\rho)$. It is easy to see that the estimate (4.2) ($\Delta_1(t) \leqslant \Delta_2(t)$)

Table 2

$\tau_s = 0.1$	$\delta_v = \|v_h - v_\infty\|_L$	10^{-2}	10^{-3}	10^{-4}	10^{-5}
	T_{theory}	0.504217	0.903755	1.300533	1.698690
	$\Delta t = 10^{-3}$	0.498	0.897	1.3	1.695
	$\Delta t = 5 \cdot 10^{-4}$	0.4975	0.895	1.2975	1.6925
	$\Delta t = 10^{-4}$	0.4965	0.8937	1.2959	1.6902
	$\Delta t = 5 \cdot 10^{-5}$	0.49645	0.89355	1.29565	1.68995
	$\Delta t = 10^{-5}$	0.49634	0.89341	1.29547	1.68973
	$\Delta t = 5 \cdot 10^{-6}$	0.496335	0.893385	1.29545	1.689705
$\tau_s = 0.25$	$\delta_v = \|v_h - v_\infty\|_L$	10^{-2}	10^{-3}	10^{-4}	10^{-5}
	T_{theory}	0.371692	0.769849	1.168006	1.566164
	$\Delta t = 10^{-3}$	0.31	0.663	1.019	1.414
	$\Delta t = 5 \cdot 10^{-4}$	0.309	0.661	1.018	1.411
	$\Delta t = 10^{-4}$	0.3083	0.66	1.0165	1.4093
	$\Delta t = 5 \cdot 10^{-5}$	0.3082	0.6599	1.0163	1.4091
	$\Delta t = 10^{-5}$	0.30815	0.65976	1.01613	1.4089
	$\Delta t = 5 \cdot 10^{-6}$	0.30814	0.65975	1.016115	1.408885
$\tau_s = 0.4$	$\delta_v = \|v_h - v_\infty\|_L$	10^{-2}	10^{-3}	10^{-4}	10^{-5}
	T_{theory}	0.082234	0.480392	0.878549	1.276707
	$\Delta t = 10^{-3}$	0.031	0.214	0.409	0.61
	$\Delta t = 5 \cdot 10^{-4}$	0.0305	0.2135	0.407	0.608
	$\Delta t = 10^{-4}$	0.0302	0.2125	0.4056	0.6068
	$\Delta t = 5 \cdot 10^{-5}$	0.0302	0.21245	0.40545	0.60675
	$\Delta t = 10^{-5}$	0.03015	0.21234	0.40539	0.60673
	$\Delta t = 5 \cdot 10^{-6}$	0.030145	0.21233	0.405385	0.606734

Table 3

	$t = 0.005$	$t = 0.01$	$t = 0.015$	$t = 0.02$	$t = 0.025$	$t = 0.03$
Δ_1	$1.107 \cdot 10^{-2}$	$4.107 \cdot 10^{-3}$	$1.526 \cdot 10^{-3}$	$5.673 \cdot 10^{-4}$	$2.107 \cdot 10^{-4}$	$7.803 \cdot 10^{-5}$
Δ_2	$1.141 \cdot 10^{-2}$	$4.252 \cdot 10^{-3}$	$1.585 \cdot 10^{-3}$	$5.906 \cdot 10^{-4}$	$2.201 \cdot 10^{-4}$	$8.205 \cdot 10^{-5}$

holds for all values of t. (The computations were performed for different values of τ_s; the data in Table 3 are given for $\tau_s = 0.05$.) The graphs corresponding to Table 3 are not presented, because the curves practically coincide. The obtained results confirm, on the one hand, that the computations are correct, and on the other hand, are close to the theoretical estimate (4.2). Thus, the transition to the steady-state mode indeed occurs exponentially with exponent $(-\mu\lambda_0/\rho)$.

4.2.2. Flow cessation. The viscoplastic medium flow cessation in ducts was studied in the recent papers [16, 17]. Note that the numerical simulation in these papers was performed only for pipes of circular and annular cross-sections, which is a simpler case (the one-dimensional problem). The numerical computations followed one of the regularized models, namely, the Papanastasiou model. For problems about the flow cessation, the drawbacks of regularized models become most obvious, because they give a qualitatively false result: the velocity decreases with time but still remains nonzero and the flow lasts infinitely long. In [16, 17], for the stopping criterion the authors took the condition that the discharge is small: $Q = \int\limits_\Omega v\,dx < 10^{-5}$. In [16, 17], the authors noted the following drawbacks.

(1) For large and medium values of the yield strength τ_s, the theoretical estimate (4.1) is satisfied; for small values of τ_s, the computed stopping time exceeds the upper bounds of the theoretical estimate,

Table 4

	$\tau_s = 10^{-4}$	$\tau_s = 10^{-3}$	$\tau_s = 10^{-2}$	$\tau_s = 0.1$	$\tau_s = 0.15$	$\tau_s = 0.2$	$\tau_s = 0.25$
T_{comp}	1.4149	1.0178	0.6196	0.2219	0.1526	0.1046	$6.933 \cdot 10^{-2}$
T_{theory}	1.4415	1.0433	0.6445	0.2402	0.1673	0.1157	$7.687 \cdot 10^{-2}$

Table 5

	$\tau_s = 10^{-4}$	$\tau_s = 10^{-3}$	$\tau_s = 0.01$	$\tau_s = 0.05$	$\tau_s = 0.1$	$\tau_s = 0.15$
T_{comp}	0.1826	0.1306	$7.259 \cdot 10^{-2}$	$3.1536 \cdot 10^{-2}$	$1.4521 \cdot 10^{-2}$	$5.872 \cdot 10^{-2}$
T_{theory}	0.1941	0.135	$7.581 \cdot 10^{-2}$	$3.36 \cdot 10^{-2}$	$1.54 \cdot 10^{-2}$	$6.015 \cdot 10^{-2}$

Table 6

	$\tau_s = 10^{-4}$	$\tau_s = 10^{-3}$	$\tau_s = 10^{-2}$	$\tau_s = 0.1$	$\tau_s = 0.15$	$\tau_s = 0.2$	$\tau_s = 0.25$
T_{comp}	0.3606	0.2646	0.1506	0.03423	0.01557	$4.965 \cdot 10^{-3}$	$2.76 \cdot 10^{-4}$
T_{theory}	0.3889	0.2723	0.1554	0.03673	0.01668	$5.140 \cdot 10^{-3}$	$2.796 \cdot 10^{-4}$

and, as was already noted, it is impossible to get rid of this drawback even by decreasing the parameter of regularization.

(2) As the pressure difference decreases instantaneously to $C_1 < C^{\text{cr}}$ ($C_1 \neq 0$), the flow velocity decreases gradually and then enters a new steady-state regime, corresponding to the new value C_1, while the viscoplastic medium must be already at rest.

In addition, the authors noted the following unexpected effect: for a large value of τ_s, a stagnant zone appears on the boundary of the disk. The authors thought that this was a computational error due to the regularization of the constitutive relations.

Thus, since the regularized models are simplifications of the initial model, for the problem under study, they realize the behavior of a nonlinear viscous fluid rather than of a viscoplastic medium. The solution given in the present paper is free from these drawbacks: the stopping time is below the theoretical upper bound for the whole range of τ_s variations (see Tables 4–6). The following three domains, for which the values of the constants contained in the stopping time estimate (4.1) are known, were considered: the disk, annulus, and square. For all the domains, the pressure difference C was set to be equal to 1. In Table 4, the stopping time of the viscoplastic medium is given for the disk of unit radius. The first row of this table presents the computed stopping time, the second row, the theoretical upper bound according to (4.1). We observe the predicted law: as the yield stress τ_s increases, the rigid zones increase, the velocity and discharge decrease, and the medium flow cessation occurs faster. Similar data are given in Table 5 for the annulus with outer $R_2 = 1$ and inner $R_1 = \frac{1}{2}$ radii (the eccentricity is $k = \frac{1}{2}$); in Table 6, similar data are given for the unit square. It is possible to see that the estimate is satisfied for a wide range of values of the yield stress, including small values. The upper bound for the stopping time depends on the density, viscosity, yield stress, and minimal eigenvalue of the Laplace operator for a given domain (the pipe cross-section). The dependence of the computed stopping time on ρ, μ, and τ_s was also investigated.

Tables 7 and 8 show how the stopping time depends on the density. In Table 7, the computations were performed for a circular pipe of unit radius for $\mu = 1$ and $\tau_s = 0.25$; in Table 8, for the unit square for $\mu = 1$ and $\tau_s = 0.15$. In both tables, the first column presents the computed time, the second, the theoretical estimate, which demonstrates practically linear dependence; the computed time also linearly depends on the density. In Tables 9 and 10, we present the stopping time dependence on the viscosity. Table 9 corresponds to a circular pipe of radius 1 and $\rho = 1$ and $\tau_s = 0.25$. Table 10, corresponds to a square with side 1 and $\rho = 1$ and $\tau_s = 0.15$. The theoretical estimate for almost all values of μ gives the inverse proportionality, which is slightly violated for $\mu = 0.01$. The computed stopping time also demonstrates the inverse proportionality with minimal deviations.

Let us consider the flow in a circular pipe in more detail. In Fig. 4, we present the velocity profiles for the cessation of a viscous fluid flow (a) and a viscoplastic medium flow for $\tau_s = 0.2$ (b) and $\tau_s = 0.4$ (c). In the case of viscous medium, we see the well-known parabolic profiles of the Poiseuille flow. The profiles

Table 7

ρ	Δt	T_{comp}	T_{theory}
0.01	10^{-7}	$6.932 \cdot 10^{-4}$	$7.688 \cdot 10^{-4}$
0.1	10^{-6}	$6.932 \cdot 10^{-3}$	$7.688 \cdot 10^{-3}$
0.2	10^{-6}	$1.386 \cdot 10^{-2}$	$1.537 \cdot 10^{-2}$
0.5	10^{-6}	$3.465 \cdot 10^{-2}$	$3.844 \cdot 10^{-2}$
1	10^{-5}	$6.930 \cdot 10^{-2}$	$7.688 \cdot 10^{-2}$
2	10^{-5}	0.1386	0.1537
5	10^{-5}	0.3465	0.3844
10	10^{-5}	0.6930	0.7688
100	10^{-4}	6.9304	7.6887

Table 8

ρ	Δt	T_{comp}	T_{theory}
0.01	10^{-7}	$1.569 \cdot 10^{-4}$	$1.683 \cdot 10^{-4}$
0.1	10^{-6}	$1.572 \cdot 10^{-3}$	$1.683 \cdot 10^{-3}$
0.2	10^{-6}	$3.141 \cdot 10^{-3}$	$3.367 \cdot 10^{-3}$
0.5	10^{-6}	$7.847 \cdot 10^{-3}$	$8.419 \cdot 10^{-3}$
1	10^{-5}	$1.572 \cdot 10^{-2}$	$1.683 \cdot 10^{-2}$
2	10^{-5}	$3.141 \cdot 10^{-2}$	$3.367 \cdot 10^{-2}$
5	10^{-5}	$7.847 \cdot 10^{-2}$	$8.419 \cdot 10^{-2}$
10	10^{-5}	0.15689	0.16838
100	10^{-4}	1.5689	1.6838

Table 9

μ	Δt	T_{comp}	T_{theory}
0.01	10^{-4}	6.9311	7.6887
0.1	10^{-5}	0.6931	0.7688
0.2	10^{-5}	0.3465	0.3844
0.5	10^{-5}	0.1386	0.1537
1	10^{-5}	$6.932 \cdot 10^{-2}$	$7.688 \cdot 10^{-2}$
2	10^{-6}	$3.464 \cdot 10^{-2}$	$3.844 \cdot 10^{-2}$
5	10^{-6}	$1.385 \cdot 10^{-2}$	$1.537 \cdot 10^{-2}$
10	10^{-6}	$6.925 \cdot 10^{-3}$	$7.688 \cdot 10^{-3}$
100	10^{-7}	$6.861 \cdot 10^{-4}$	$7.688 \cdot 10^{-4}$

in Figs. 4 *b* and 4 *c* have a flat piece at the center, which corresponds to the flow core increasing with time. Figure 4 *c* corresponds to a larger value of the yield stress, and hence the velocity is less and the rigid zone dimension is greater. The upper profiles correspond to steady-state flows. Figure 4 *b* presents the velocity profiles at times $t = 0,\ 0.02,\ 0.04,\ 0.06,\ 0.08,\ 0.1$; Fig. 4 *c*, at times $t = 0, 0.002, 0.004, 0.006, 0.008, 0.01$. The lower profiles, in addition ro the core at the center ($r = 0$), have a small plane piece near the boundary, i.e., the stagnant zones appear. Figures 5–7 show the time evolution of the rigid zones. Figure 5 corresponds to $\tau_s = 0.1$: $t = 0\,(a)$, $t = 0.2\,(b)$, $t = 0.21\,(c)$, and $t = 0.22\,(d)$; Fig. 6 corresponds to $\tau_s = 0.2$: $t = 0\,(a)$, $t = 0.08\,(b)$, $t = 0.1\,(c)$, and $t = 0.103\,(d)$; and Fig. 7 corresponds to $\tau_s = 0.3$: $t = 0\,(a)$, $t = 0.035\,(b)$, $t = 0.041\,(c)$, and $t = 0.0425\,(d)$. In these figures, it is clearly seen that the flow

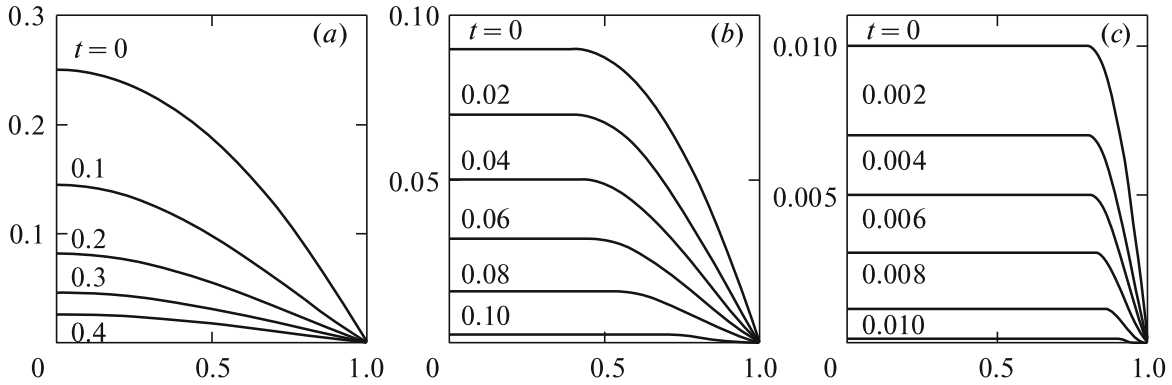

Fig. 4.

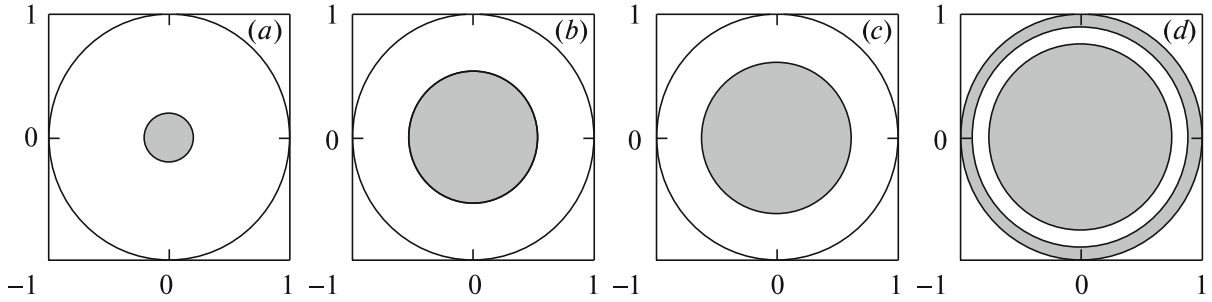

Fig. 5.

Table 10

μ	Δt	T_{comp}	T_{theory}
0.01	10^{-4}	1.4902	1.5938
0.1	10^{-5}	0.15695	0.16838
0.2	10^{-5}	$7.849 \cdot 10^{-2}$	$8.419 \cdot 10^{-2}$
0.5	10^{-5}	$3.142 \cdot 10^{-2}$	$3.367 \cdot 10^{-2}$
1	10^{-5}	$1.572 \cdot 10^{-2}$	$1.683 \cdot 10^{-2}$
2	10^{-6}	$7.825 \cdot 10^{-3}$	$8.419 \cdot 10^{-3}$
5	10^{-6}	$3.117 \cdot 10^{-3}$	$3.367 \cdot 10^{-3}$
10	10^{-6}	$1.547 \cdot 10^{-3}$	$1.683 \cdot 10^{-3}$
100	10^{-7}	$1.348 \cdot 10^{-4}$	$1.683 \cdot 10^{-4}$

cores grow at the disk center and stagnant zones appear on disk boundary at the end of the flow shortly before the flow cessation. Thus, for unsteady flows, the obtained results confirm the effect of appearance of stagnant zones, which was discovered for larger values of τ_s in [16].

In Fig. 8, we present the volume velocity profiles for a viscoplastic medium with $\tau_s = 0$ in the stationary case (a), at times $t = 0.05$ (b), and at times $t = 0.102$ (c). For the steady-state flow, the surface looks like an inverted cup, for the flow at time $t = 0.05$, like a truncated cone, for the flow before cessation, like a cylinder. The value of the velocity for $t = 0.102$ decreases almost by two orders of magnitude, the plane core occupies almost the entire disk, and the flow of the deformed medium occurs only in a thin layer between the core and the annular stagnant zone on the boundary. In Fig. 9, we present the graphs for the velocity variations at the center in the course of time for $\tau_s = 0.1, 0.2, 0.3, 0.4$. For large values of the yield stress $\tau_s = 0.3, 0.4$, the velocity at the center is smaller, the medium cessation occurs faster, and the dependence of $v_c(t)$ on time is almost linear. The velocity $v_c(t)$ for $\tau_s = 0.1, 0.2$ is closer to the exponential dependence, and the decrease in the velocity at the center gradually becomes slower.

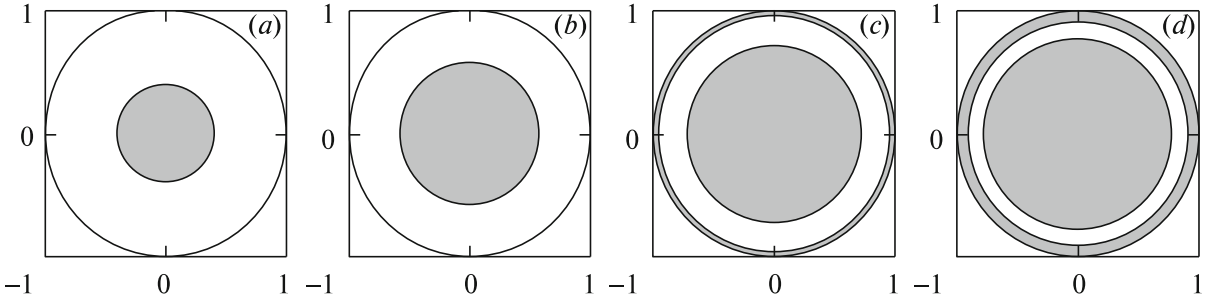

Fig. 6.

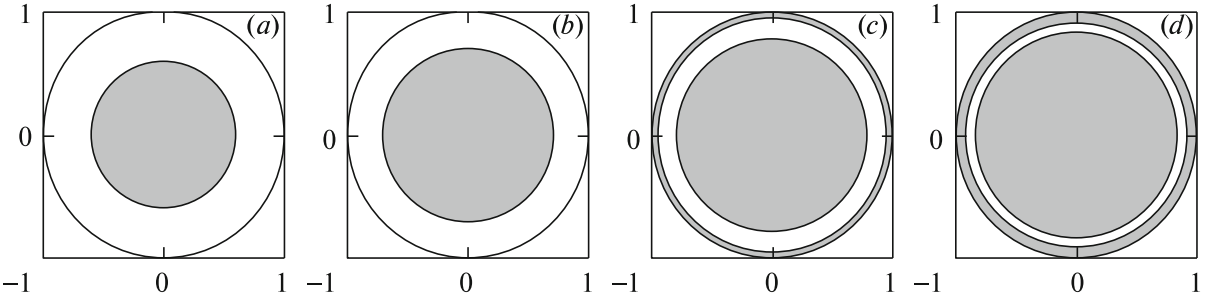

Fig. 7.

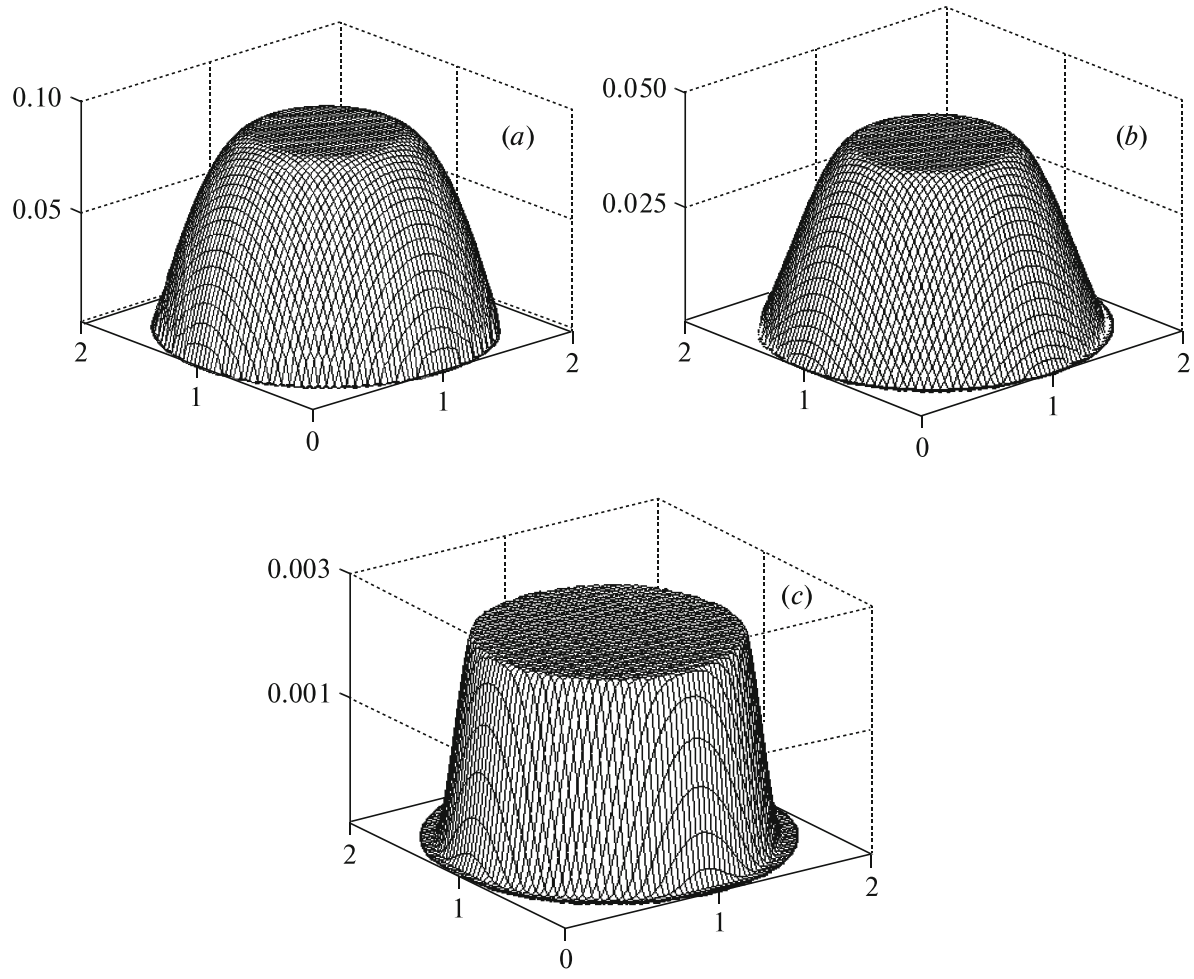

Fig. 8.

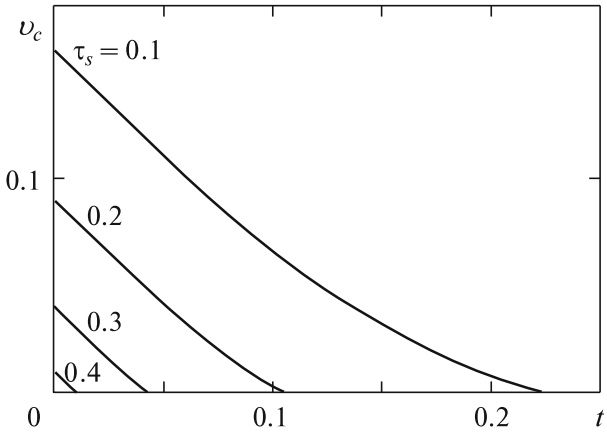

Fig. 9.

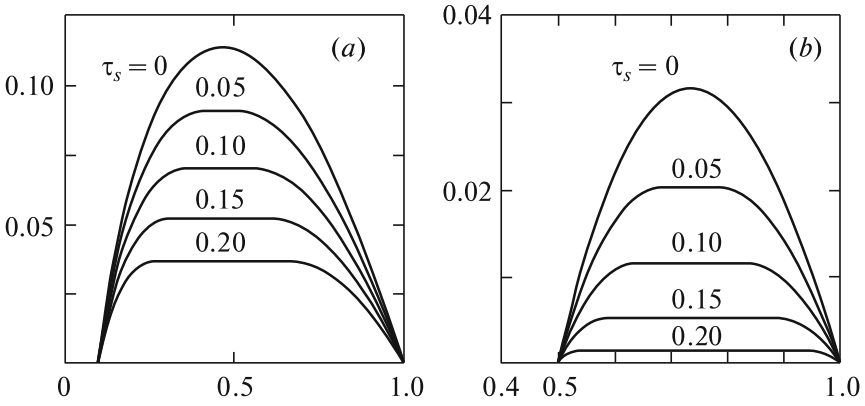

Fig. 10.

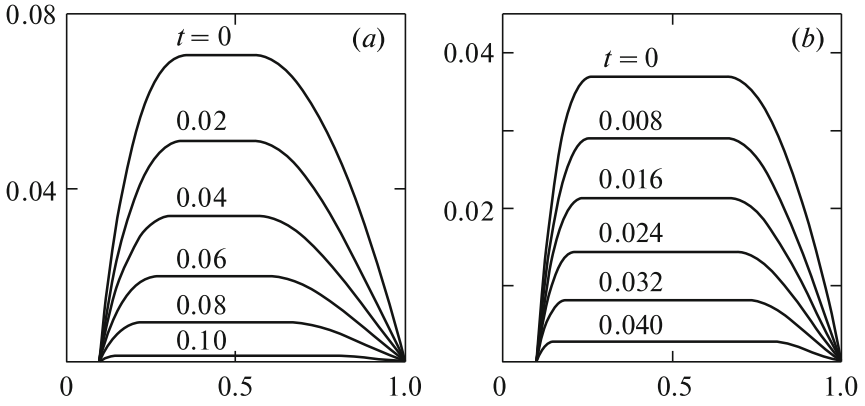

Fig. 11.

Consider the medium flow in an annulus with outer radius $R = 1$ and the pressure gradient $C = 1$. In Fig. 10, we construct the velocity profiles for steady-state flows for $k = 0.5$ and $k = 0.1$ for different values of the yield stress. They completely correspond to the analytic solution. The dimension of rigid zones noticeably increases with increasing τ_s, and the profiles become more and more plane. For smaller eccentricity ($k = 0.1$), the profiles become more asymmetric and slightly inclined to the internal boundary. The velocity profiles for the flow cessation in an annular pipe are given in Fig. 11; for $k = 0.1$ and $\tau_s = 0.1$ at times $t = 0$, 0.02, 0.04, 0.06, 0.08, 0.1, in Fig. 11 *a*, and for $k = 0.1$ and $\tau_s = 0.2$ at times $t = 0$, 0.008, 0.016, 0.024, 0.032, 0.04, in Fig. 11 *b*. In Fig. 12, we present the distribution of

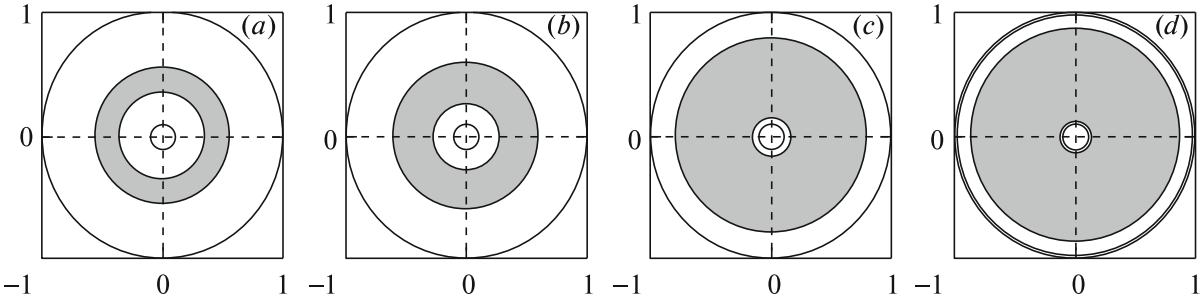

Fig. 12.

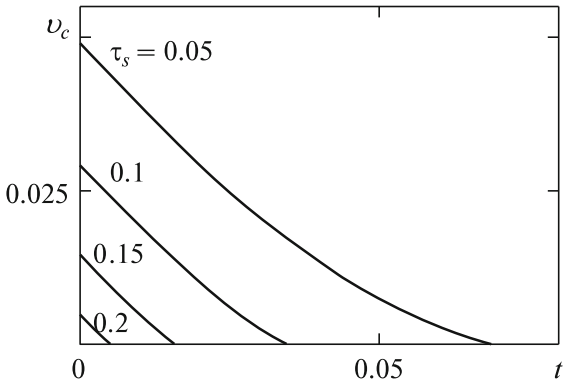

Fig. 13.

rigid zones, which corresponds to $k = 0.1$ and $\tau_s = 0.1$ and times $t = 0\,(a)$, $t = 0.06\,(b)$, $t = 0.1\,(c)$, and $t = 0.1038\,(d)$. We note that a stagnant zone appears on the outer boundary of the annulus not long before the cessation $T_{\text{stop}} = 0.1047$. The stagnant zones on the boundary of the annulus with $k = 0.1$ also appear for other values of the yield stress. For a fixed value $\tau_s = 0.1$, we considered the annular cross-sections with the outer radius 1 and the eccentricities $k = 0.1,\ 0.2,\ 0.3,\ 0.4,\ 0.5$. For $k = 0.1,\ 0.2,\ 0.3$, the stagnant zones appeared, for $k = 0.4,\ 0.5$, they did not appear. Possibly, an appropriate choice of the yield stress for given k will allow us to discover this effect, but the authors did not pursue this goal. The solution of the problem of flow cessation in an annular gap was studied in detail in [17]. The obtained solution is in a very good agreement with that obtained in [17], and hence we do not pay attention to the flow in an annular gap any more. We only note that, in [17], the stagnant zones were not found and the stopping time was not estimated for small values of τ_s. Our solution agrees with this estimate for τ_s in a wide range of values; the results are given in Table 5.

The problem of flow cessation in a square or rectangular duct is much more interesting. For the initial condition we take the steady-state solution. Figure 13 illustrates the velocity time variation at the center for $\tau_s = 0.05,\ 0.1,\ 0.15,\ 0.2$ (the cross-section is the unit square). The medium behavior is similar to the above-described flow in a circular duct (Fig. 9). In Fig. 14, we present the velocity profiles for the unit square for $\tau_s = 0.1$ along the median cross-section and along the diagonal cross-section at times $t = 0,\ 0.01,\ 0.02,\ 0.03,\ 0.0346$. In the course of time, the profiles become more plane, the rigid cores increase, the stagnant zones appear on the boundary, and moreover, they appear not only on the diagonal but are also noticeable in the median cross-section; thus, the flow region separates from the duct walls. In Fig. 15, we present the evolution of rigid zones for $\tau_s = 0.1$ and $t = 0\,(a)$, for $\tau_s = 0.1$ and $t = 0.02\,(b)$, for $\tau_s = 0.1$ and $t = 0.03\,(c)$, and for $\tau_s = 0.1$ and $t = 0.0346\,(d)$. At the initial time moment, there is a small core of the flow at the center and practically unnoticeable stagnant zones at the corners. Further, the rigid zones increase, and it is possible to note a rather fast increase in stagnant zones. In this case, the earlier unknown characteristic of stagnant zones, which is typical precisely of the unsteady flow, begins to manifest itself: shortly before the complete deceleration (the flow cessation occurs at $T_{\text{stop}} = 0.0348$), the stagnant zone surrounds the entire boundary contour and the flow region in strictly inside the domain Ω. Recall that in the stationary case the flow region must be adjacent to

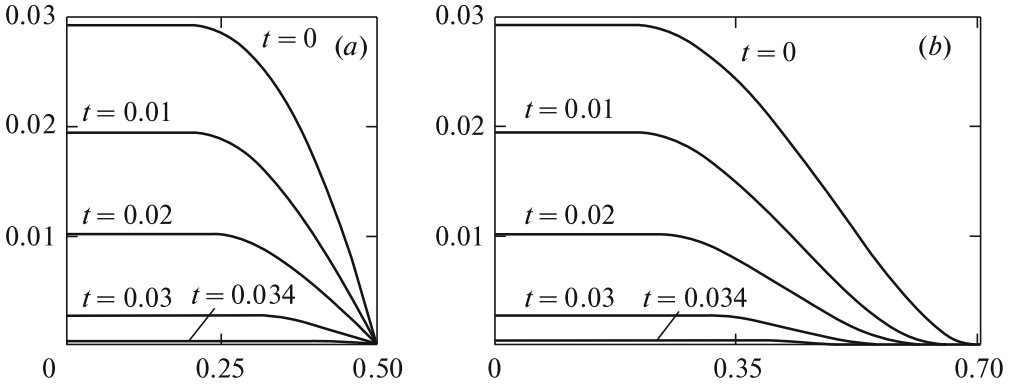

Fig. 14.

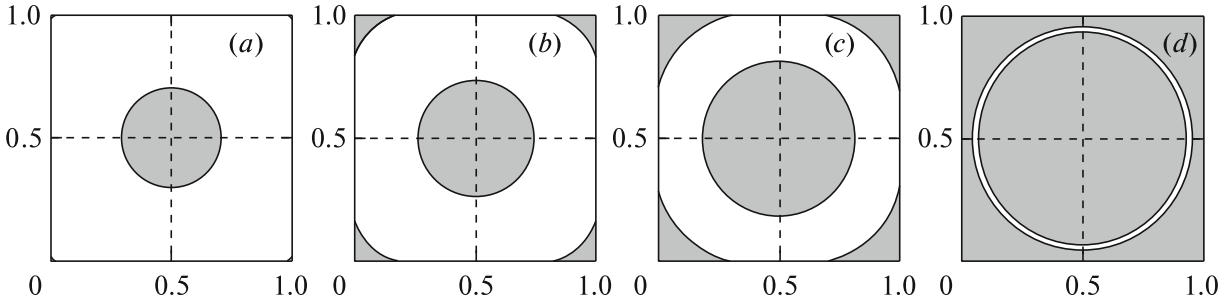

Fig. 15.

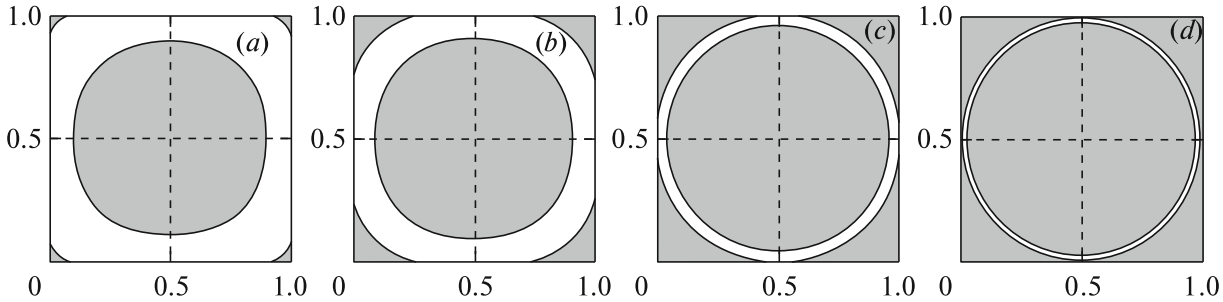

Fig. 16.

the boundary and the stagnant zones are at the corners and cannot be outside the critical curve L (Fig. 2). We note that in Figs. 14 *a* and 14 *b*, the velocity profile at time $t = 0.0346$ practically coincides with the abscissa axis, while in Fig. 15 *d*, one can see that the motion still occurs. For $\tau_s = 0.2$, the evolution of rigid zones is shown in Fig. 16 at the time moments $t = 0$ (*a*), $t = 0.003$ (*b*), $t = 0.004$ (*c*), and $t = 0.0048$ (*d*) (the flow cessation occurs at $T_{\text{stop}} = 0.00498$). Qualitatively, the flow is like that in the preceding case, and the stagnant zone also surrounds the boundary contour not long before the cessation.

It is of interest to compare the flow in a closed duct, where the velocity is equal to zero on the boundary, with the flow in a duct with open upper cover. We assume that the upper free surface is horizontal. The distribution of rigid zones in times ($\tau_s = 0.1$) is shown in Fig. 17. At the lower corners of the cross-section, a stagnant zone is formed, and it fills the duct bottom in the course of time. The flow core is adjacent to the free surface at the center, and to the left and right of it, there is a deformable medium. In Table 11, we compare the stopping time for the flow in the closed duct with that in the open duct for various values of the yield stress. The flow is the open duct lasts longer then that in the closed duct, which is natural, because the flow velocity in the open duct is greater. For $\tau_s = 0.25$, the stopping times

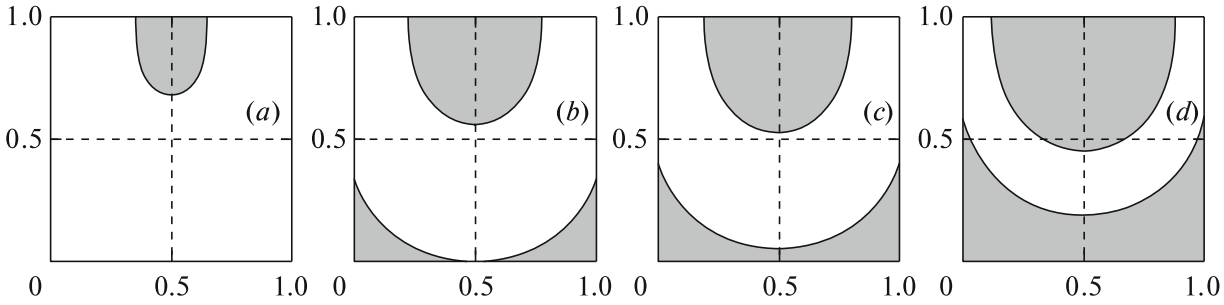

Fig. 17.

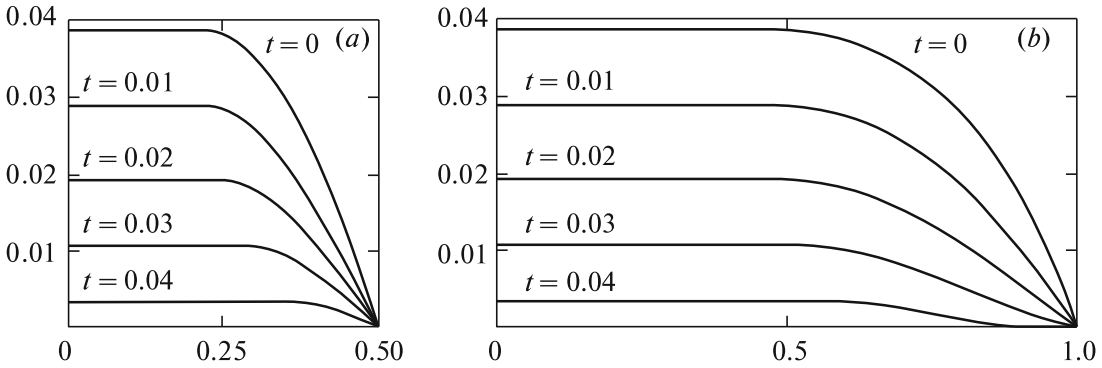

Fig. 18.

Table 11

	$\tau_s = 10^{-4}$	$\tau_s = 10^{-3}$	$\tau_s = 10^{-2}$	$\tau_s = 0.1$	$\tau_s = 0.15$	$\tau_s = 0.2$	$\tau_s = 0.25$
T_{close}	0.3606	0.2646	0.1506	0.0342	0.0155	$4.965 \cdot 10^{-3}$	$2.76 \cdot 10^{-4}$
T_{open}	0.5377	0.4316	0.2615	0.0772	0.0455	0.0246	0.0107

differ significantly, because this value is close to the limit value $\tau_s^{\text{cr}} = 0.27$ and the flow velocity in the closed duct is very small.

In Fig. 18, we present the velocity profiles for the rectangle $\Omega = [0, 2] \times [0, 1]$ for $\tau_s = 0.15$ along the transverse (a) and longitudinal (b) cross-sections at times $t = 0$, 0.01, 0.02, 0.03, 0.04. In Figs. 19 and 20, we show the time evolution of rigid zones for the rectangle $\Omega = [0, 2] \times [0, 1]$ for $\tau_s = 0.15$ and $\tau_s = 0.25$, respectively. For $\tau_s = 0.15$, the time evolution of rigid zones is presented at the time moments: $t = 0\,(a)$, $t = 0.03\,(b)$, $t = 0.04\,(c)$, and $t = 0.044\,(d)$ and the flow cessation occurs at $t = 0.0447$. As was already noted, in the stationary case, there exist a curve L, which separates the domain outside of which the stagnant zones cannot exist. For the unsteady flow in a rectangle, starting from a time moment, the stagnant zone completely surrounds the narrow sides of the rectangle, and the flow region is adjacent to the wide sides of the rectangle. Figure 21 illustrates the flow deceleration process in the rectangular duct $\Omega = [0, 4] \times [0, 1]$ for $\tau_s = 0.25$. This flow is similar to those described above, the comparison with Fig. 21 is of interest, because $\tau_s = 0.25$ and $C = 1$ in both of these cases. If we compare the steady-state flows ($t = 0$), then we see that the stagnant zones are somewhat less for the $[4 \times 1]$ rectangle; the flow core is more elongated and narrower; the velocity is larger than that in the $[2 \times 1]$ rectangle.

For the unsteady flow, the stopping time is T_{stop}=0.0238 for the larger cross-section and T_{stop}=0.0108 for the smaller cross-section. These laws are preserved for further elongation of the rectangle.

Just as in the stationary problem, we studied how the cross-section geometry affects the stopping time for the flow. For the fixed yield stress $\tau_s = 0.1$ and the flow rate $Q = 0.0179$ fixed at the initial time moment, we considered the flows in pipes for different side ratios ε. The results of this study are given in

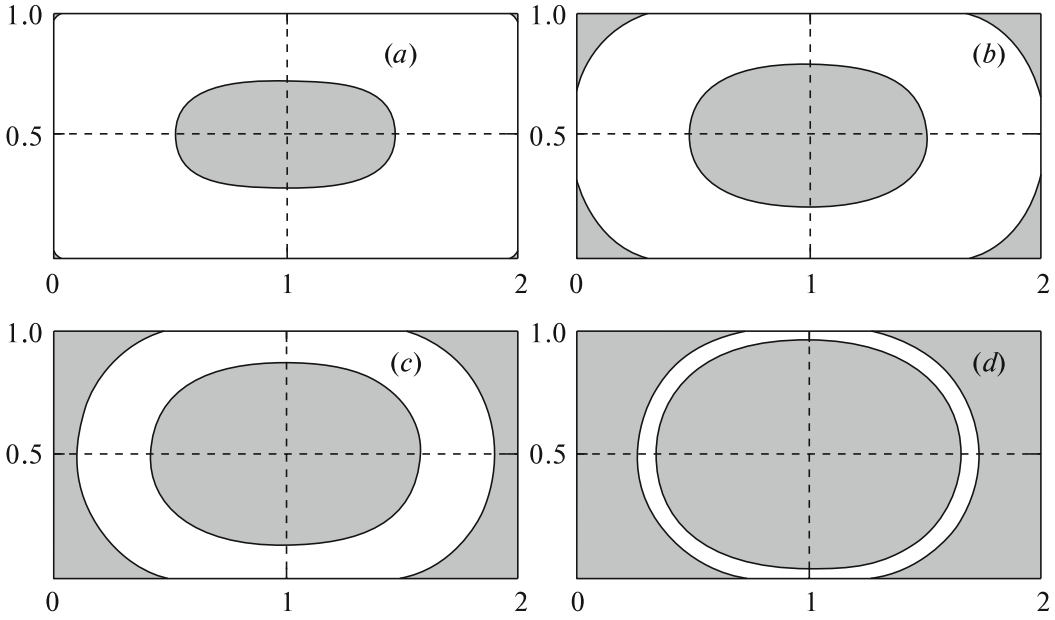

Fig. 19.

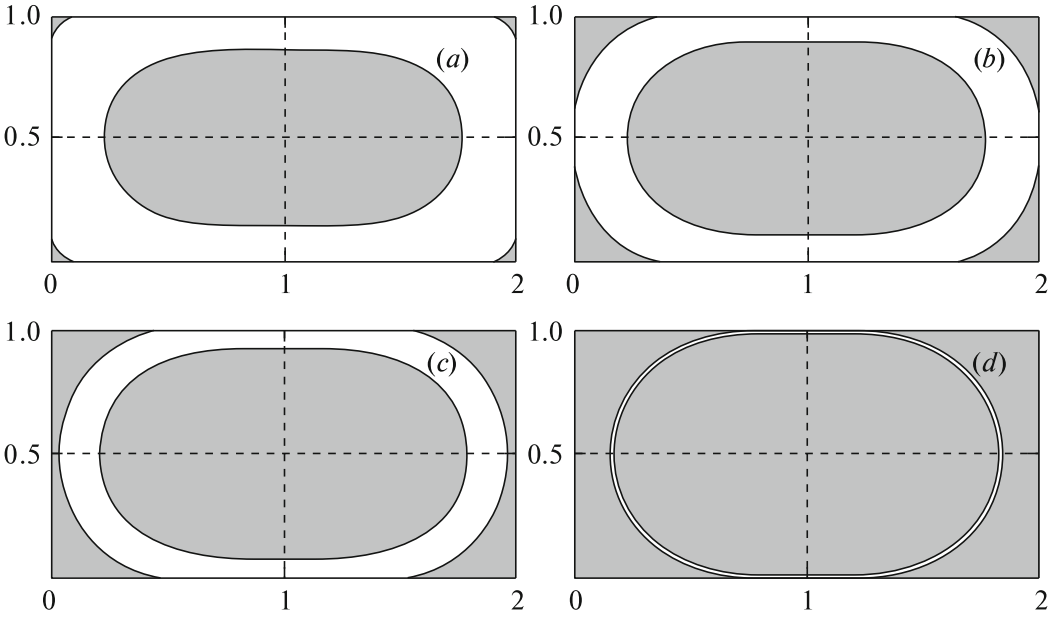

Fig. 20.

Table 12

	$\varepsilon = 1$	$\varepsilon = 2$	$\varepsilon = 3$	$\varepsilon = 4$	$\varepsilon = 5$	$\varepsilon = 10$
T_{comp}	0.03442	0.02997	0.02545	0.02181	0.01910	0.01211
T_{theory}	0.03672	0.03239	0.02738	0.02364	0.02086	0.01357

Table 12. The flow in the square pipe was the longest. The more elongated the cross-section, the faster the medium cessation occurs.

4.2.3. Flow cessation for a nonzero pressure gradient. Consider a steady-state flow in a duct under the action of the pressure gradient C. Then the gradient instantaneously drops to $C_1 < C^{\text{cr}}$. According to (4.1), the flow must stop in finite time $T \leqslant T_{\text{theory}}$. In Fig. 22, we present the velocity dependence $v_h(t)$

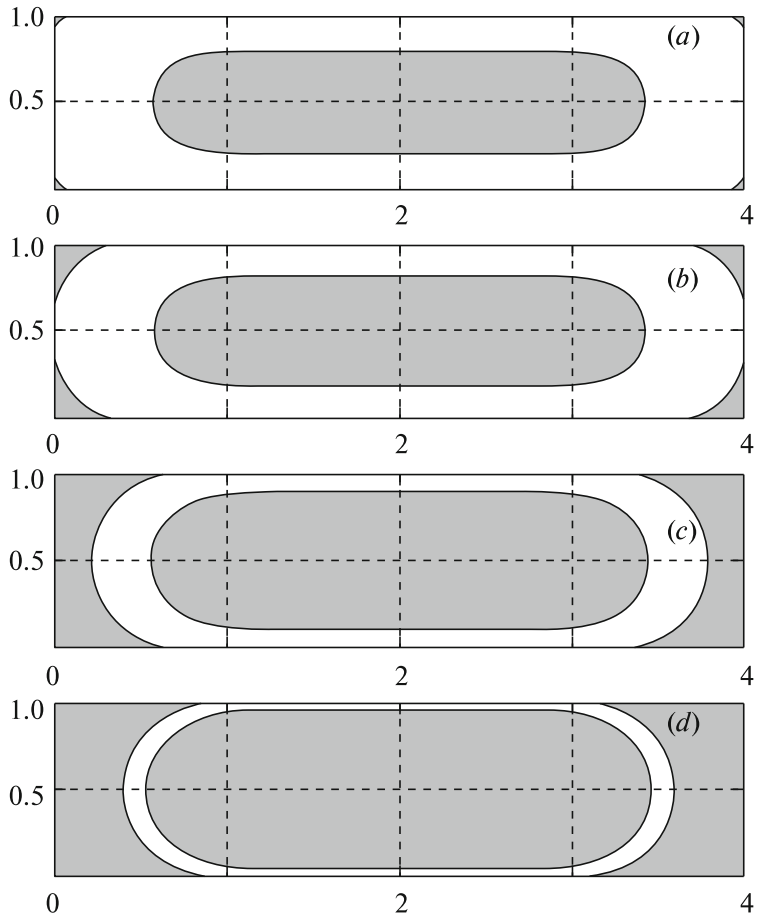

Fig. 21.

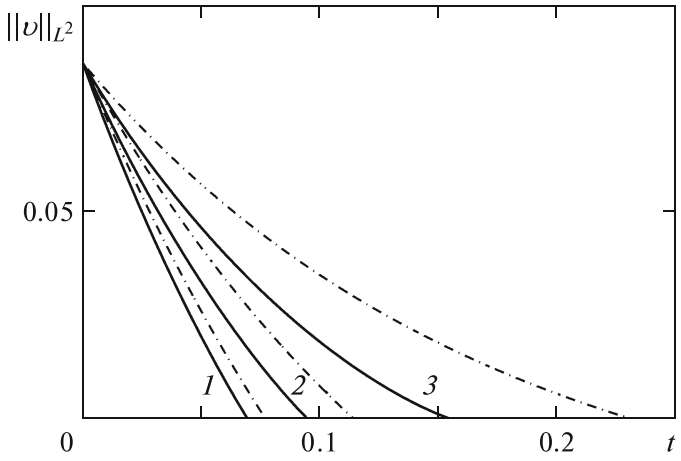

Fig. 22.

in the $L^2(\Omega)$-norm for a flow of a viscoplastic medium with $\tau_s = 0.25$ in a circular pipe of unit radius for $C = 1$ and $C^{\mathrm{cr}} = 0.5$. Curve *1* corresponds to cessation at $C_1 = 0$, curve *2*, at $C_1 = 0.2$, curve *3*, at $C_1 = 0.4$, and the dashed lines correspond to the theoretical estimate (4.1). In all these cases, the medium cessation occurred and the graphs of $\|v_h(t)\|_{L^2(\Omega)}$ lie below the estimation graphs.

A similar problem was solved for a square pipe of unit area for the yield stress $\tau_s = 0.15$. In Fig. 3 *b*, this problem is associated with the interval $t \geqslant 0.03$. First, the flow is accelerated from the immovable

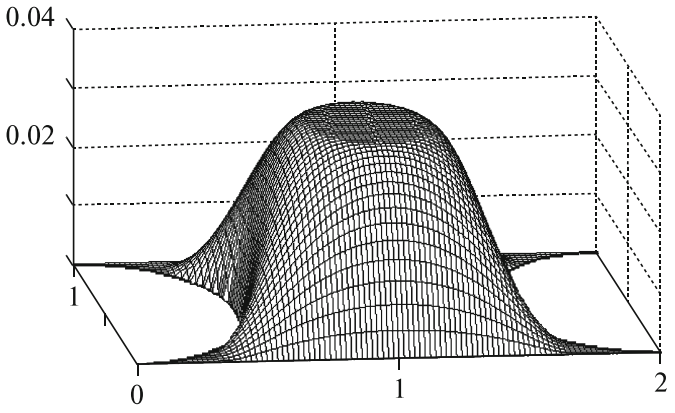

Fig. 23.

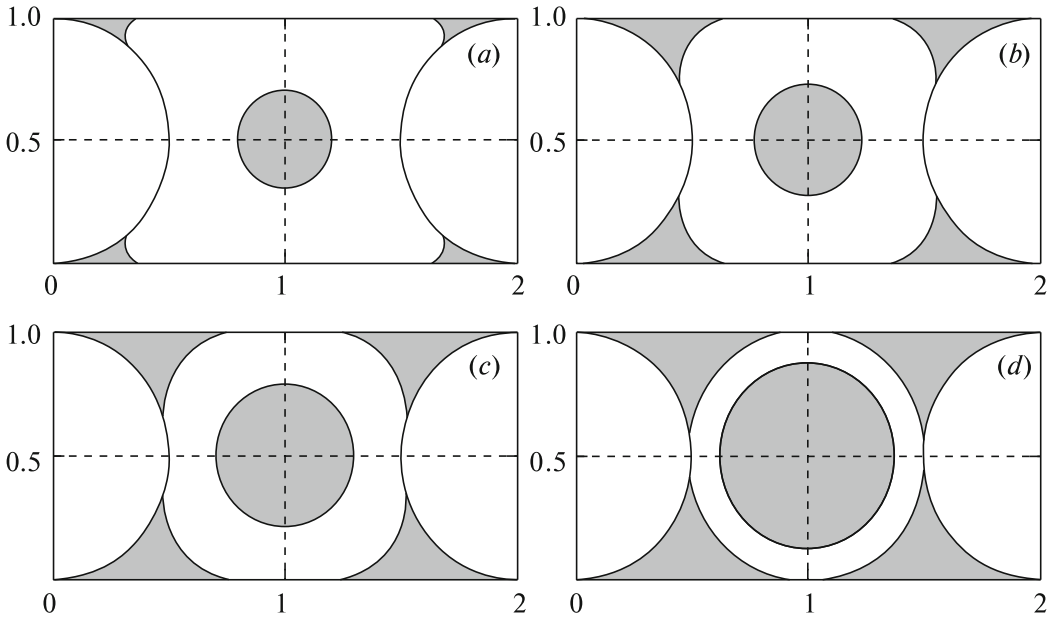

Fig. 24.

state to the steady-state regime, which corresponds to $C = 1$, and at $t = 0.03$, the pressure gradient instantaneously drops to C_1. In the first case, $C_1 = 0$, in the second, $C_1 = 0.1$ ($C^{\rm cr} = 0.27$). In both of these cases, the medium cessation occurs, and the theoretical estimate (4.1), shown by dashed lines, was satisfied. The other values $C < C^{\rm cr}$ were also considered. A similar picture was observed: the flow cessation occurred, the computed value of $\|v_h(t)\|_{L^2(\Omega)}$ was lower than the theoretical estimate. As $f \to C^{\rm cr}$, the difference between the computed and estimated times increased.

4.3. Domains of Complicated Shape

It is of great interest to consider the solution of this problem in domains of complicated shape, both in the stationary and nonstationary cases.

1. A rectangle with a semicircular cut. The domain is a rectangle with dimension $a \times b$, $a > b$, with semicircles of radius $\frac{1}{2}b$ cut away. In Fig. 23, we show the spatial profile of the cross-section in the stationary case ($a = 2$, $b = 1$). The distribution of rigid zones is predictable in the stationary case: the stagnant zones are at the acute corners, and the flow core is at the center. The picture corresponds to the yield stress $\tau_s = 0.1$. As the yield stress increases, the rigid zones also increase and the flow velocity decreases. Figure 24 demonstrates the time evolution of rigid zones: $t = 0\,(a)$, $t = 0.02\,(b)$, $t = 0.03\,(c)$, and $t = 0.036\,(d)$. The stopping time is $T_{\rm stop} = 0.0375$.

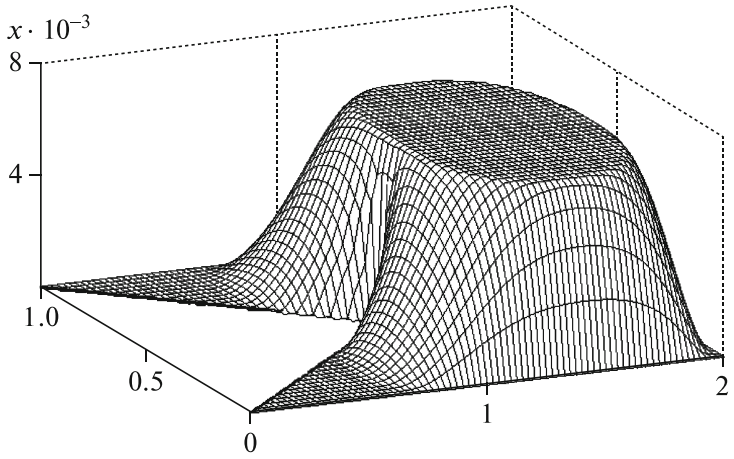

Fig. 25.

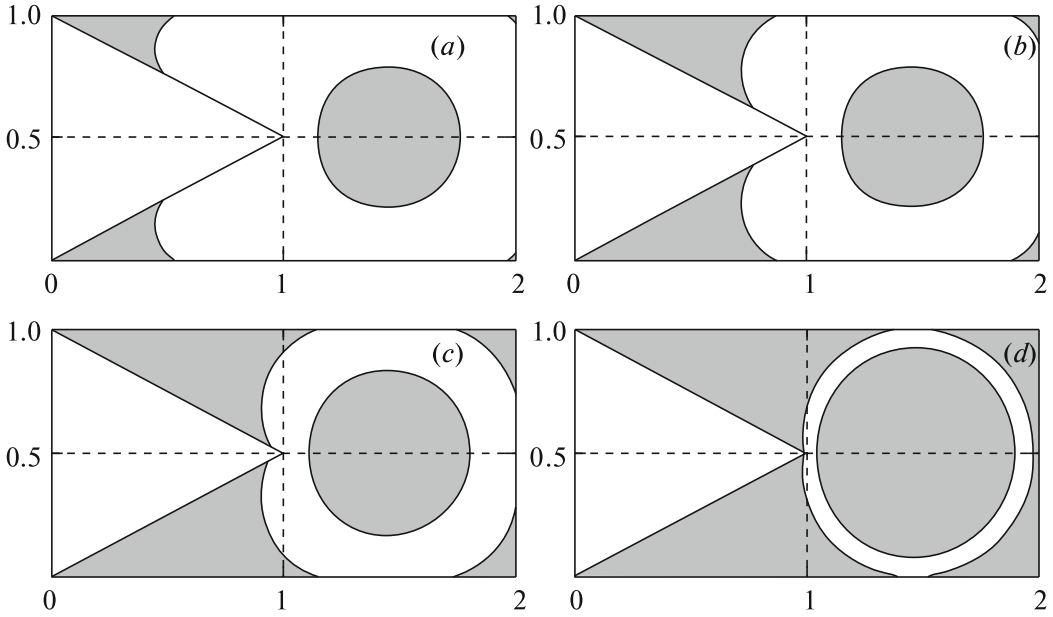

Fig. 26.

2. A "small flag". The spatial profile is shown in Fig. 25; the distribution of rigid zones in the stationary case is shown in Fig. 26*a*. Small stagnant zones are at the right corners of the main part of the flag, just as in the case of a square or a rectangle, large stagnant zones are at the acute corners of the "tails" of the domain, and the flow core is in the interior of the domain. There are no singularities at the vertex of the reentering angle. The flow corresponds to the yield stress $\tau_s = 0.15$. In Fig. 26, the rigid zones are shown at time $t = 0$ (*a*), $t = 0.004$ (*b*), $t = 0.014$ (*c*), and $t = 0.018$ (*d*). In the course of time, the rigid zones increase and, not long before the flow cessation, the larger part of the "flag" is occupied by the stagnant zone with a thin annular region of the deformable medium and the circular core of the flow.

3. A sand glass. The domain is of dimension $[1.08 \times 2]$, and the bridge width is equal to 0.8. The domain with two axes of symmetry is obtained by partial intersection of two isosceles triangles. The spatial profile of the flow is shown in Fig. 27, the picture of rigid zones in given in Fig. 28: $t = 0$ (*a*), $t = 0.007$ (*b*), and $t = 0.009$ (*c*). At the outer corners and at the center, there are stagnant zones, and the flow cores are at the triangle centers. This domain is an interesting example of a homogeneous medium with two flow cores. Examples of several cores (joint flow of two viscoplastic fluids with different yield stresses in a duct) can be found in [13, 15].

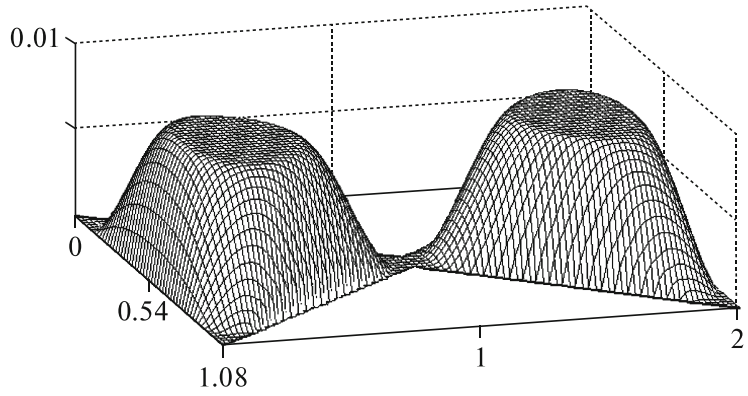

Fig. 27.

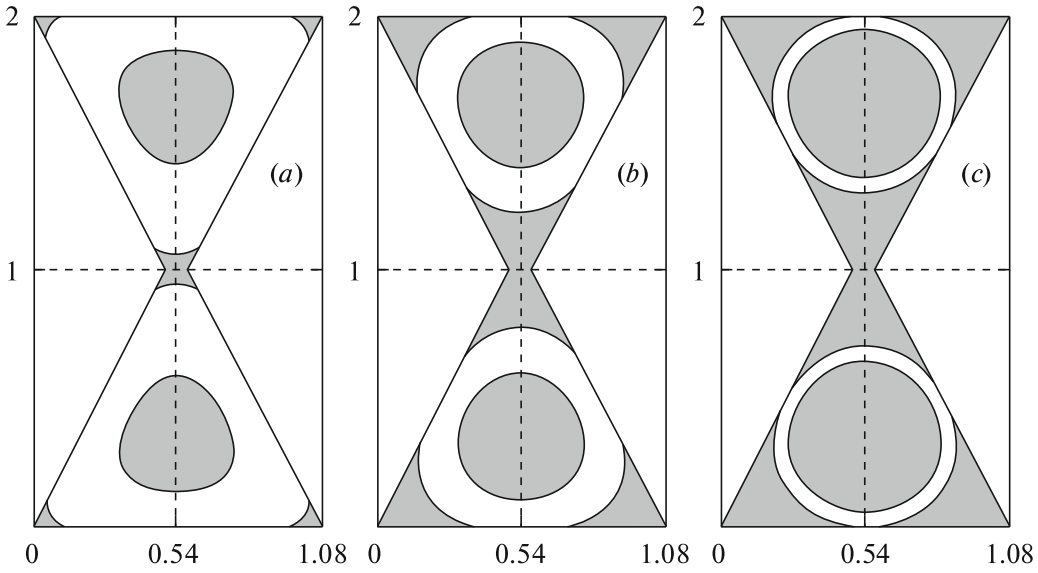

Fig. 28.

5. CONCLUSION

We numerically solved problems of Bingham–Il'yushin medium flow in ducts of different cross-section. We studied how the medium internal parameters such as the yield stress, density, viscosity, and the cross-section geometric characteristics affect the flow character. The results thus obtained are in complete agreement with the theoretical estimates [2]. We also compared our results with the results obtained by other authors by using the regularized models; the results obtained in the present paper correctly describe the viscoplastic medium behavior. We noted the earlier unknown qualitative singularities of unsteady regimes; namely, not long before the flow cessation, stagnant zones completely surrounding the boundary contour (disk, annulus, square) may appear; moreover, the stagnant zones go outside the critical curves surrounding the stagnant zones in the steady flow. The solutions obtained for some domains of complicated shape were obtained for the first time, in both the stationary and nonstationary cases. We also considered a flow with a homogeneous yield stress in a simply-connected domain, which has two flow cores.

ACKNOWLEDGMENTS

The authors thank R. V. Goldstein for valuable remarks and advice, which helped significantly to improve the paper.

The research was in part financially supported by the Russian Foundation for Basic Research, projects nos. 08-01-00353a and 09-01-00565a.

REFERENCES

1. D. M. Klimov, A. G. Petrov, and D. V. Georgievskii, *Viscoplastic Flows: Dynamical Chaos, Stability, Mixing* (Nauka, Moscow, 2005) [in Russian].
2. E. J. Dean, R. Glowinski, and G. Guidoboni, "On the Numerical Simulation of Bingham Visco-Plastic Flow: Old and New Results," J. Non-Newtonian Fluid Mech. **142** (1–3), 36–62 (2007).
3. O. B. Magomedov and B. E. Pobedrya, "Certain Problems of Viscoelastoplastic Flow," in *Elasticity and Non-Elasticity*, No. 4 (Izd-vo MGU, Moscow, 1975), pp. 152–169 [in Russian].
4. R. V. Goldstein and V. M. Entov, *Qualitative Methods in Continuum Mechanics* (Nauka, Moscow, 1989; Wiley, New York, 1994).
5. P. P. Mosolov and V. P. Miasnikov, "Variational Methods in the Theory of the Fluidity of a Viscous-Plastic Medium," Prikl. Mat. Mekh. **29** (3), 468–492 (1965) [J. Appl. Math. Mech. (Engl. Transl.) **29** (3), 545–577 (1965)].
6. P. P. Mosolov and V. P. Miasnikov, "On Stagnant Flow Regions of a Viscous-Plastic Medium in Pipes," Prikl. Mat. Mekh. **30** (4), 705–717 (1966) [J. Appl. Math. Mech. (Engl. Transl.) **30** (4), 841–854 (1966)].
7. P. P. Mosolov and V. P. Miasnikov, "On Qualitative Singularities of the Flow of a Viscoplastic Medium in Pipes," Prikl. Mat. Mekh. **31** (3), 581–585 (1967) [J. Appl. Math. Mech. (Engl. Transl.) **31** (3), 609–613 (1967)].
8. G. Duvaut and J.-L. Lions, *Les Inéquations en Mécanique et Physique* (Dunod, Paris, 1972; Nauka, Moscow, 1980).
9. I. Ekeland and R. Temam, *Convex Analysis and Variational Problems* (North-Holland, Amsterdam, 1976; Mir, Moscow, 1979).
10. A. G. Petrov and L. V. Cherepanov, "Exact Solutions of the Problem of Unsteady Flow of a Viscoplastic Medium in a Circular Pipe," Izv. Akad. Nauk. Mekh. Zhidk. Gaza, No. 2. 13–24 (2003) [Fluid Dyn. (Engl. Transl.) **38** (2), 175–185 (2003)].
11. R. Glowinski, J.-L. Lions, and R. Trémolières, *Analyse Numérique des Inéquations Variationnelles* (Dunod, Parix, 1976; Mir, Moscow, 1979).
12. N. Roquet and P. Saramito, "An Adaptive Finite Element Method for Viscoplastic Fluid Flows in Pipes," Comput. Meth. Appl. Mech. Eng. **190** (40), 5391–5412 (2001).
13. M. A. Moyers-Gonzalez and I. A. Frigaard, "Numerical Solution of Duct Flows of Multiple Visco-Plastic Fluids," J. Non-Newtonian Fluid Mech. **122** (1–3), 227–241 (2004).
14. R. R. Huilgol and Z. You, "Application of the Augmented Lagrangian Method to Steady Pipe Flows of Bingham, Casson, and Herschel-Bulkley Fluids," J. Non-Newtonian Fluid Mech. **128** (2–3), 126–143 (2005).
15. E. A. Muravleva, "Finite-Difference Schemes for the Computation of Viscoplastic Medium Flows in a Channel," Mat. Modelirovanie, No. 12, 76–88 (2008) [Math. Models Comput. Simul. (Engl. Transl.) **1** (6), 768–779 (2009)].
16. M. Chatzimina, G. C. Georgiou, I. Argyropaidas, et al., "Cessation of Couette and Poiseuille Flows of a Bingham Plastic and Finite Stopping Times," JNNFM **129** (3), 117–127 (2005).
17. M. Chatzimina, C. Xenophontosa, G. C. Georgiou, et al. "Cessation of Annular Poiseuille Flows of Bingham Plastics," JNNFM **142** (1–3), 135–142 (2007).
18. H. Zhu and D. De Kee, "A Numerical Study of Couette Flow of Non-Newtonian Fluids with a Yield Stress," J. Non-Newtonian Fluid Mech. **143** (2–3), 64–70 (2007).
19. V. P. Beskachko, O. A. Golovnya, and A. E. Korenchenko, "Numerical Model of Nonstationary Flow of a Viscoplastic Fluid in a Rotational Viscosimeter," Inzh. Fiz. Zh., No. 1, 12–14 (2007) [J. Engng Phys. Thermophys. (Engl. Transl.) **80** (1), 11–14 (2007)].
20. A. E. Korenchenko, V. P. Beskachko, and O. A. Golovnya, "Possibility of Identifying the Viscoplastic Properties of Liquids in Experiments with an Oscillating-Cup Viscometer," Zh. Prikl. Mekh. Tekh. Fiz. **47** (6), 59–63 (2006) [J. Appl. Mech. Tech. Phys. (Engl. Transl.) **47** (6), 821–824 (2006)].
21. A. A. Il'yushin, "Deformation of Viscoplastic Bodies," Uchen. Zap. MGU. Mekh. **39**, 3–81 (1940).
22. P. P. Mosolov, "Variational Methods in Nonstationary Problems (Parabolic Case)," Izv. Akad. Nauk SSSR. Ser. Mat. **34** (2), 425–457 (1970). [Math. USSR Izv. (Engl. Transl.) **4** (2), 431–463 (1970)],
23. M. Fortin and R. Glowinski, *Augmented Lagrangian Methods: Applications to the Numerical Solution of Boundary-Value Problems* (North-Holland, Amsterdam, 1983).
24. E. A. Muravleva, "Solution of a Nonstationary Problem for the Bingham Medium on the Basis of Evolutional Variational Inequalities," in *7th All-Russian Seminar "Grid Methods in Boundary-Value Problems and Applications* (Kazan, 2007), pp. 213–218 [in Russian].
25. E. A. Muravleva, "The Problem of Stopping the Flow of a Viscoplastic Medium in a Channel," Vestnik Moskov. Univ. Ser. I. Mat. Mekh., **64** (1), 67–70 (2009) [Moscow Univ. Mech. Bull. (Engl. Transl.) **64** (1), 25–28 (2009)].
26. G. I. Marchuk, *Splitting Methods* (Nauka, Moscow, 1988) [in Russian].